Heliyon 8 (2022) e11080

Contents lists available at ScienceDirect

Heliyon

journal homepage: www.cell.com/heliyon

Research article

Bryophyllum pinnatum mediated synthesis of zinc oxide nanoparticles: characterization and application as biocontrol agents for multi-drug-resistant uropathogens

Renu Jagdish, Kiran Nehra *

Department of Biotechnology, Deenbandhu Chhotu Ram University of Science and Technology, Murthal 131039, Haryana, India

HIGHLIGHTS

- Identification and characterization of multi-drug-resistant (MDR) uropathogenic bacteria.
- Fabrication of ZnO nanoparticles (NPs) using phytochemicals of *Bryophyllum pinnatum* for reduction and stabilization.
- Physiochemical characterization of biosynthesized ZnO NPs using FTIR, XRD, SEM, EDX, HR-TEM, and Zeta potential.
- Evaluation of the antimicrobial potential of synthesized ZnO NPs against clinical MDR uropathogenic bacterial isolates for their use as alternative therapeutic agents for UTIs.

GRAPHICAL ABSTRACT

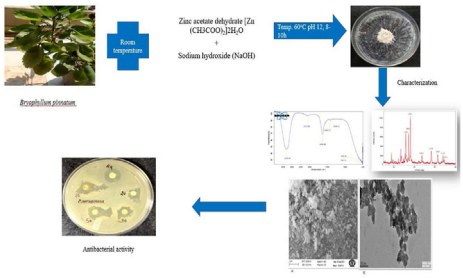

ARTICLE INFO

Keywords:
Antimicrobial activity
Bryophyllum leaf extract
MDR
UTI
ZnO nanoparticles

ABSTRACT

The emerging era of antimicrobial resistance has become a challenge for the potentiality of current antibiotic therapy, making the treatment of several diseases, including urinary tract infections (UTIs) very chaotic. To combat the present circumstances, there is an urge among the scientific community to find efficient substitutes for antibiotic therapy, which may potentially delimit the antimicrobial resistance among the various uropathogens. In this direction, the upcoming field of nanotechnology holds a high potential. Therefore, the present study aimed at the evaluation of the antimicrobial potential of green synthesized zinc oxide nanoparticles. The nanoparticles were synthesized using *Bryophyllum pinnatum* plant leaf extract and were characterized with the help of several analytical techniques. A sharp peak obtained at 369 nm by UV-Visible spectroscopy affirmed the synthesis of Bryophyllum- ZnO nanoparticles, and the FTIR spectroscopy confirmed the conjugation of different phytochemicals. XRD analysis revealed the crystallinity and hexagonal conformation, and through SEM and HR-TEM, the particle size of the synthesized Bryophyllum- ZnO nanoparticles was found to be between 14-35 nm. The synthesized green nanoparticles, when tested against a few highly MDR uropathogenic bacteria (*E. coli, E. furgusonii, K. pneumoniae, S. flexneri,* and *P. aeruginosa*), were observed to exhibit high antimicrobial response (zones of inhibition ranging between 22 mm to 28 mm), thus confirming that these were bestowed with potent antimicrobial ability. Hence, from the present work, it could be concluded that Bryophyllum- ZnO nanoparticles can be used as potential nanoantibiotic sources to deal with UTIs.

* Corresponding author.
E-mail address: kirannehra.bt@dcrustm.org (K. Nehra).

https://doi.org/10.1016/j.heliyon.2022.e11080
Received 28 April 2022; Received in revised form 3 August 2022; Accepted 10 October 2022

1. Introduction

Nanoparticles (NPs) are miniature particles exhibiting a high surface area with a volume ratio that upsurges their activity towards adjoining particles. This characteristic of nanoparticles has fascinated the scientific community to explore their remarkable properties for applications in several fields, including the health sector, food technology, drug delivery, cosmetics, optical science, etc. [1, 2, 3]. Nanoparticles have also been bestowed with antibacterial and antioxidant properties, leading to their terminology as "nano-antibiotics".

Generally, chemical, physical and biological methods have been employed to produce nanoparticles. But the chemical and physical practices have certain limitations, *viz.* usage of toxic and lavish chemicals, prolonged pressure and temperature conditions, longer periods of reflux reaction, and release of toxic by-products that are not eco-friendly. Therefore, biological methods are more fascinating to the research community, as these involve the usage of natural microorganisms (including bacteria, algae, and fungi), enzymes, yeast, and plants, instead of harmful chemicals [4, 5, 6]. However, among these, the use of plants, which is commonly termed as the green synthesis methodology, is getting more attention recently. This methodology is inexpensive, less time-consuming, capable of synthesis at a large scale, releases only non-toxic by-products, and results into good stability of the synthesized nanoparticles [5, 7]. The plant phytochemicals play a pivotal role as capping agents in nanoparticle synthesis and stabilization, the stabilization of nanoparticles being crucial for their practical functionality [5, 8]. Plant phytochemicals in plant extracts stabilize the nanoparticles by various mechanisms that include van der Waals, hydration, electrostatic, and steric stabilization [9].

In the present times, among the various metal nanoparticles undergoing research at different stages, the green chemistry of zinc oxide (ZnO) NPs is considered more attractive, since ZnO has been enlisted as GRAS (generally recognized as safe) metal oxide by the US FDA [2]. These NPs are bestowed with various biomedical applications, including antibacterial, antifungal, anti-inflammatory, anti-diabetic, drug delivery ability, and anticancer and antioxidant properties. Besides these, ZnO NPs also possess the following properties: piezoelectricity, optical transparency, non-toxicity, electric conductivity, wide availability, and better stability. Due to these properties, they have wide applications in solar cells, catalysis, varnishes, laser, optoelectronic devices, plastics, and pharmaceuticals, especially in cosmetics, including sunscreen, where these act as protecting agents possessing UV filtering ability [10, 11, 12]. Although bestowed with several beneficial properties, as elaborated above, studies related to the application of these NPs as antibacterials to treat infectious diseases spread by multi-drug resistant (MDR) bacteria are minimal.

UTIs have been considered the most commonly mistreated and the second most common contagious disease following pneumonia [13, 14]. More recently, it has become a serious health problem among human beings, accounting for nearly 150 million cases annually throughout the world, which costs an excessive burden on the global economy, amounting to approximately US $6 billion [15, 16]. Further, an upsurge in antimicrobial resistance among UTI causing pathogens has made its empiric antibiotic therapy ineffective. This has led to an increase in the rate of mortality and morbidity globally, which has further resulted in a rapid rise and spread of multidrug-resistant (MDR) uropathogens, *viz. Escherichia coli, Klebsiella pneumonia* and *Pseudomonas aeruginosa* [17, 18, 19, 20]. To encounter this ever-rising problem of multi-drug resistance, nanotechnology seems to be a spectacular field of science capable of delimiting the problem of antimicrobial resistance among uropathogens by exploiting tiny nanoparticles at their best efficacies [21, 22].

Bryophyllum pinnatum (family: Crassulaceae) plant is a succulent herb, commonly called life leaf and air plant, grown as an ornamental garden plant in America, India, China, etc. It has been reported that this plant is used to treat various ailments like high blood pressure, burn heal, and kidney stones. It has also been found to be bestowed with multiple activities, *viz.,* anticonvulsant, antioxidant, antimicrobial, analgesic, nephroprotective, anti-diabetic, antihelminthic, neuropharmacological and antipyretic [23, 24], hence the plant possesses several beneficial properties. In the present study, its phytochemicals have been exploited to explore their potential as an alternative treatment for highly multi-drug-resistant (MDR) uropathogens. The plant leaf extract has been employed as a capping, stabilizing, and reducing agent to synthesize ZnO nanoparticles. To the best of our knowledge, the present study is the first of its kind describing the synthesis of ZnO NPs from *Bryophyllum pinnatum* leaf extract for its potential use as an antibacterial agent for the treatment of UTI caused by MDR uropathogens.

2. Materials and methodology

2.1. Collection of clinical bacterial uropathogens

Eight clinical uropathogenic bacterial isolates were collected from different pathology laboratories, including Park Nidaan Hospital Sonipat, Frank Institute of Medical Sciences (FIMS) Sonipat, and Hari Pathology Laboratory, in Sonipat district of Haryana state in India.

2.2. Morphological, biochemical and molecular characterization of collected clinical uropathogenic bacterial isolates

All the collected uropathogenic isolates were subjected to morphological, biochemical and molecular analysis for their identification and characterization. The collected clinical bacterial strains were purified by repeated streaking, and were then phenotypically identified using Gram's staining [25]. Biochemical characterization was carried out through standard biochemical tests (IMViC), including the Indole test, Methyl Red test, Voges-Proskauer test and Simmon's Citrate test [14]. For molecular identification, fresh 24h bacterial culture of each purified bacterial isolate was used for the extraction of genomic DNA of the bacteria using a DNA purification kit (Wizard® Genomic DNA Purification Kit, Promega India). The genomic DNA of each bacterium was subjected to 16S rRNA gene amplification with the aid of universal primers [27F as forward primer (5′AGAGTTTGATCCTGGCTCAG3′) and 1492R as the reverse primer (5′GGTTACCTTGTTACGACTT3′)]. The reaction mixture (25μl) and amplification conditions were set up as detailed in Table 1. After amplification, the PCR products were visualized by running in 1% agarose gel for 60 min at 100V, and were further subjected to sequencing from AgriGenome Labs Pvt. Ltd. Kochi, Kerala.

2.3. Antibiotic susceptibility analysis of the clinical uropathogenic isolates

The collected clinical uropathogenic bacterial isolates were further examined for antibiotic susceptibility profiling against a set of 23 different antibiotics generally used for the treatment of UTI, including Ampicillin, Cefadroxil, Cefoperazone/sulbactam, Cefotaxime, Cefuroxime, Ceftriaxone, Ceftazidime, Imipenem, Meropenem, Amoxicillin-

Table 1. Details of PCR working and thermal cycling conditions.

PCR working conditions	
Master mix 2X (Promega)	14 μl
27F & 1492R	1.5 μl each
Template DNA	2 μl
PCR water	6 μl
Total reaction volume	25 μl
PCR thermal cycling conditions	
Initial denaturation	94 °C for 3 min
Denaturation	94 °C for the 60 s (35 cycles)
Annealing	55 °C for the 30 s
Final extension	72 °C for 10 min

Table 2. Phenotypic, biochemical, and molecular characterization of uropathogenic bacterial isolates.

S.No.	Isolate Name	Gram's Staining	IMViC Test				Molecular Identification	
			Indole Test	Methyl red	Voges-Proskauer Test	Simmons citrate Test	Identification as per BLAST	Assigned Gen Bank Accession Number
1	F26	Negative	Negative	Negative	Positive	Positive	*Klebsiella pneumoniae*	MT444767
2	F32	Negative	Positive	Positive	Negative	Negative	*Escherichia furgusonii*	MT444768
3	H33	Negative	Negative	Negative	Positive	Positive	*Klebsiella pneumoniae*	MT444769
4	N39	Negative	Negative	Positive	Negative	Negative	*Shigella flexneri*	MT444770
5	N40	Negative	Negative	Negative	Positive	Positive	*Klebsiella pneumoniae*	MT444771
6	P27	Negative	Negative	Negative	Negative	Positive	*Pseudomonas aeruginosa*	MT444772
7	H42	Negative	Negative	Negative	Positive	Positive	*Klebsiella pneumoniae*	MT444773
8	H11	Negative	Positive	Positive	Negative	Negative	*Escherichia coli*	OK035230

clavulanate, Ampicillin/sulbactam, Piperacillin/tazobactam, Ciprofloxacin, Levofloxacin, Ofloxacin, Amikacin, Gentamycin, Netilmicin, Nitrofurantoin, Tigecycline, Colistin, Cotrimoxazole, and Fosfomycin by using Kirby Bauer's disc diffusion method. All these 23 antibiotics belonged mainly to five significant classes (Beta-lactams, Beta-lactamase suppressors/inhibitors, Fluoroquinolones, Aminoglycosides, and a few other antibiotics belonging to nitrofurans, sulfonamides, glycylcycline and polymyxins) [26, 27]. Each strain's fresh 24 h culture was swabbed onto Mueller Hinton Agar (MHA) plates, and different antibiotic discs were impregnated onto the dried MHA plates, which were then incubated at 37 °C for 20–24 h. Susceptibility to various antibiotic discs was evaluated as resistant and sensitive by evaluating the diameter of the zone of inhibition as per the guidelines of the Clinical and Laboratory Standards Institute (CLSI) [28].

2.4. Collection of plant material and preparation of plant extract

The *Bryophyllum pinnatum* plant leaves were collected from the campus of Deenbandhu Chhotu Ram University of Science and Technology, Murthal. Fresh 30g green leaves of *Bryophyllum pinnatum* plant were gathered and washed multiple times in running tap water, which was further repeated with deionized water to dispose-off dirt particles. The fresh green leaves were chopped into fine fragments and soaked in an Erlenmeyer beaker containing 250 ml of double-distilled water. The mixture was boiled at 60 °–80 °C for 15–20 min on a hot magnetic stirrer plate. After boiling, a pale-yellow coloured solution was obtained, which was then cooled down at room temperature and filtered using Whatman filter paper no 1. The resultant filtrate was preserved at 4 °C for further study.

2.5. Green synthesis of ZnO nanoparticles using B. pinnatum leaf extract

A 0.01 M solution of zinc acetate dihydrate was processed in a glass bottle containing 50 ml of double-distilled water, and 25 ml of *B. pinnatum* leaf extract was supplemented to the above-prepared solution. This was followed by a dropwise addition of 2 M NaOH to the mixture of zinc acetate and plant extract for maintaining the pH at 12. The mixture was then placed at constant stirring for 90 min on a magnetic stirrer, which led to the formation of a white coloured precipitate, observed to be settled down at the bottom of the mixture. The resultant residue was isolated from the reaction mixture by centrifugation with double distilled water twice at 7,000 rpm for 7 min each. A final washing with ethanol was carried out at 7,000 rpm for 7 min to remove any impurities, or excess of plant extract. The precipitate was kept for drying at 60 °C for 8–10 h in a hot air oven to convert zinc acetate to ZnO nanoparticles. The resultant pale white coloured powder was collected and stored in tight vials for further examination.

2.6. Optimization of synthesized ZnO nanoparticles

Different abiotic parameters, including the concentration of zinc acetate, the volume of the plant extract, temperature and pH, were optimised to synthesise ZnO nanoparticles. Various concentrations of zinc acetate (0.0025 M, 0.005 M, 0.01 M, and 0.02 M) were evaluated by keeping all other parameters constant. Similarly, the optimum temperature and pH were finalized by undergoing the synthesis of zinc oxide nanoparticles at varying temperatures (40 °C, 60 °C, 80 °C, and 100 °C) and pH (8, 10, 12, and 13); however, keeping all other parameters (zinc acetate concentration, plant extract volume, and pH/temperature) constant during each synthesis reaction.

2.7. Characterization of synthesized ZnO nanoparticles

To confirm the synthesis of ZnO NPs and to determine their shape, size, and morphology, various analytical techniques, *viz.*, UV-Vis spectroscopy, Diffuse Reflectance Spectroscopy (DRS), X-ray diffraction (XRD), Fourier Transform Infra-Red (FTIR) spectroscopy, Scanning Electron Microscopy (SEM), High- Resolution Transmission Electron Microscopy (HR-TEM), and Zeta potential were performed.

2.7.1. UV-visible spectroscopy and optical absorption properties

The optical properties of ZnO nanoparticles were tested with the aid of UV-Visible spectroscopy, which is primarily based upon the absorption of UV spectra using a wavelength of 300–850 nm. UV-Vis

Table 3. Antibiotic susceptibility pattern of identified uropathogenic bacterial isolates to a set of 23 standard antibiotics.

S.No.	Isolate Name	Molecular Identification	Resistance of the isolate to the number of antibiotics	Resistance of the isolate to the number of different classes of antibiotics	Sensitivity of the isolates to the number of specific antibiotics
1	F26	*Klebsiella pneumoniae*	20	05	3
2	F32	*Escherichia furgusonii*	21	05	2
3	H33	*Klebsiella pneumoniae*	19	˃4	4
4	N39	*Shigella flexneri*	20	˃4	3
5	N40	*Klebsiella pneumoniae*	22	05	1
6	P27	*Pseudomonas aeruginosa*	20	05	3
7	H42	*Klebsiella pneumoniae*	20	05	3
8	H11	*Escherichia coli*	21	05	2

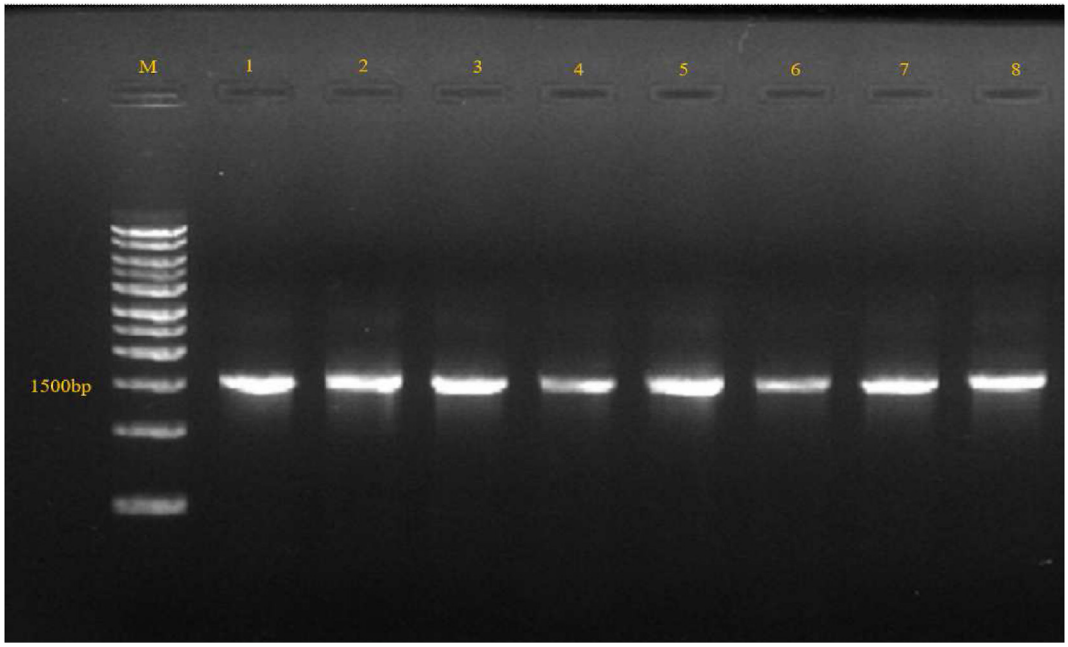

Figure 1. PCR amplification of 16S rRNA gene sequence of highly MDR uropathogenic bacterial isolates.

spectrophotometer UV-3092 (LabIndia Analytical Instruments Pvt. Ltd.) was employed for the spectroscopy, and the absorption values were plotted with the help of OriginPro 9.

Diffuse reflectance spectroscopy was carried out on LAMBDA 750 (PerkinElmer) UV-Vis NIR Spectrophotometer. A wavelength range of 300–800 nm was used to record the spectra using diffuse reflectance mode, eventually, converted into absorbance coefficient by applying Kubelka–Munk function [29]. The band gap value was examined from the plot of Kubelka–Munk function versus the energy of the absorbed light. The graphs were plotted using Origin Pro 9.

2.7.2. XRD spectroscopy

XRD scanning was performed by using X-Ray Diffractometer (Rigaku, Ultima IV) within the wavelength range of 1.20 A^{o}. The XRD scanned within the scope of 2θ of 10°–80° at 40 kV and 40 mA with a divergence slit of 0.3 mm in 2θ/θ, having a steady mode of scanning.

2.7.3. FTIR spectroscopy

FTIR spectroscopy was employed to examine the presence of organic and inorganic functionalities of plant phytochemicals that play a pivotal role in stabilizing nanoparticles. FTIR spectra for the synthesized dried

Table 4. Percentage (%) resistance of bacterial isolates to antibiotics belonging to five major classes.

S.No.	Antibiotic Class **	Name of Antibiotic*	Abbreviation used	Concentr-ation used (μg)	Number of bacterial isolates exhibiting resistance	Percentage (%) of bacterial resistance
1	Beta-lactams ❖Penicillin ❖Cephalosporins ❖Carbapenems	Ampicillin	AMP	10	08	100
		Cefadroxil	CFR	30	08	100
		Cefoperazone/sulbactam	CFS	75/10	08	100
		Cefotaxime	CTX	30	08	100
		Ceftazidime	CAZ	30	08	100
		Ceftriaxone	CTR	30	08	100
		Cefuroxime	CXM	30	08	100
		Imipenem	IMP	10	08	100
		Meropenem	MRP	10	08	100
2	Beta-lactamase suppressers	Amoxicillin-clavulanate	AMC	30	08	100
		Ampicillin/sulbactam	AS	10/10	08	100
		Piperacillin/tazobactam	PIT	100/10	08	100
3	Fluoroquinolones	Ciprofloxacin	CIP	5	08	100
		Levofloxacin	LE	5	08	100
		Ofloxacin	OF	5	08	100
4	Aminoglycosides	Amikacin	AK	30	04	50
		Gentamycin	GEN	10	08	100
		Netilmicin	NET	30	08	100
5	Others	Nitrofurantoin (Nitrofurans)	NIT	300	05	62.5
		Tigecycline (glycylcycline)	TGC	15	02	25
		Colistin (polymyxin)	CL	10	02	25
		Cotrimoxazole (sulfonamides)	COT	25	08	100
		Fosfomycin	FO	200	06	75

Note: * Total number of antibiotics used: 23; **Total number of different classes of antibiotics: 05.

nanopowder and the *Bryophyllum pinnatum* leaf extract were analyzed using FTIR (LabIndia) in the range of 4000–500 cm^{-1} by employing the Attenuated Total Reflectance technique.

2.7.4. SEM microscopy and EDX spectroscopy

Scanning electron microscopy was performed to observe the shape, morphology, and size of the synthesized nanoparticles. A diluted suspension of the synthesized nanoparticles was prepared and allowed to sonicate for 5 min. From the prepared suspension, a drop was placed on the gold grid and set to dry for 15 min, and the pattern holder was then loaded with this dried sample. SEM evaluation was performed by using ZEISS EVO 18 SEM. Energy-dispersive X-ray spectroscopy (EDX) was carried out to confirm the elemental composition of bio-synthesized ZnONPs. EDX analysis was performed with the aid of EDX-AMETEK.

2.7.5. HR-TEM microscopy

High-Resolution Transmission electron microscopy (HR-TEM) was accomplished for deciding the precise size as well as the form of the synthesized NPs. A less turbid and diluted suspension of the synthesized nanoparticles was sonicated for 5 min. A drop was positioned on the copper grid from the prepared suspension and dried for 15 min; the sample holder was then loaded with this dried sample. HR-TEM evaluation was accomplished using TELOS shiny area SA 150kx electron microscope at a high-anxiety voltage of 200 kV to depict the scale and form of NPs. An Olympus smooth imaging system was used to visualise the images.

2.7.6. Zeta potential

The surface charge potentiality of synthesized nanoparticles determines the stability of nanoparticles, and it was evaluated by using Particle Analyzer Lite Sizer 500 manufactured by Anton Paar. The analysis was carried out at 25 °C, and the result was documented as an operation of time.

2.8. Evaluation of the antimicrobial response of the synthesized nanoparticles

The bio-synthesized nanoparticles were exploited to evaluate their antimicrobial ability against eight clinical multi-drug-resistant uropathogens using antibacterial assay and further determining their minimum inhibitory concentration (MIC).

The antimicrobial ability of the bio-synthesized ZnO NPs was determined by employing the agar disc diffusion method against highly multi-drug-resistant (MDR) Gram-negative uropathogens, *viz., Escherichia coli, Escherichia furgusonii, Klebsiella pneumoniae, Pseudomonas aeruginosa, and Shigella flexneri.* Each strain's fresh 24 h bacterial culture was spread homogenously onto MHA plates. The discs with varying concentrations (20 μg/ml, 30 μg/ml, 50 μg/ml, and 70 μg/ml) of the synthesized ZnO NPs were impregnated on the surface of the plates and then placed at 37 °C for 20–24 h in an incubator. Amikacin, a standard antibiotic disc (30 μg), was also placed onto MHA plates along with ZnO NPs and it was used as the control. After completion of incubation, the level of zones produced around each disc were examined.

The bio-synthesized ZnO NPs were further evaluated for their minimum inhibitory concentration [30, 31] using the broth macro-dilution method. MIC can be delineated as the lowest concentration of the sample capable of eliciting a response against the targeted microorganism to prevent its growth. MIC establishes an inverse proportional relation to antimicrobial ability; as lower the MIC value, higher the antimicrobial activity. All the uropathogens (Table 3) were seeded overnight in nutrient broth (NB) media, and the final inoculum/suspension was maintained at 1×10^5 CFU/ml. To evaluate the MIC, 2 ml of nutrient broth (NB) was drained into sterile tubes. In the first sterile tube, 2 ml of nanoparticle suspension (256 μg/ml) was added, and in the subsequent tubes, a two-fold dilution of the nanoparticles was prepared. The last tube in the successive series containing 2 ml of media was discarded. All the tubes were implanted with 40 μl of microbial suspension and nurtured for 20–24 h at 37 °C in an incubator. The presence and absence of turbidity in the media was checked visually to determine MIC values. Further, the quantative analysis was carried-out by examining the absorbance of the various dilutions present in different tubes at OD600 nm to confirm the MIC values. Both the experiments (antibacterial activity and MIC of synthesized ZnO NPs) were performed in triplicates and the results were examined as mean ± SD (standard deviation).

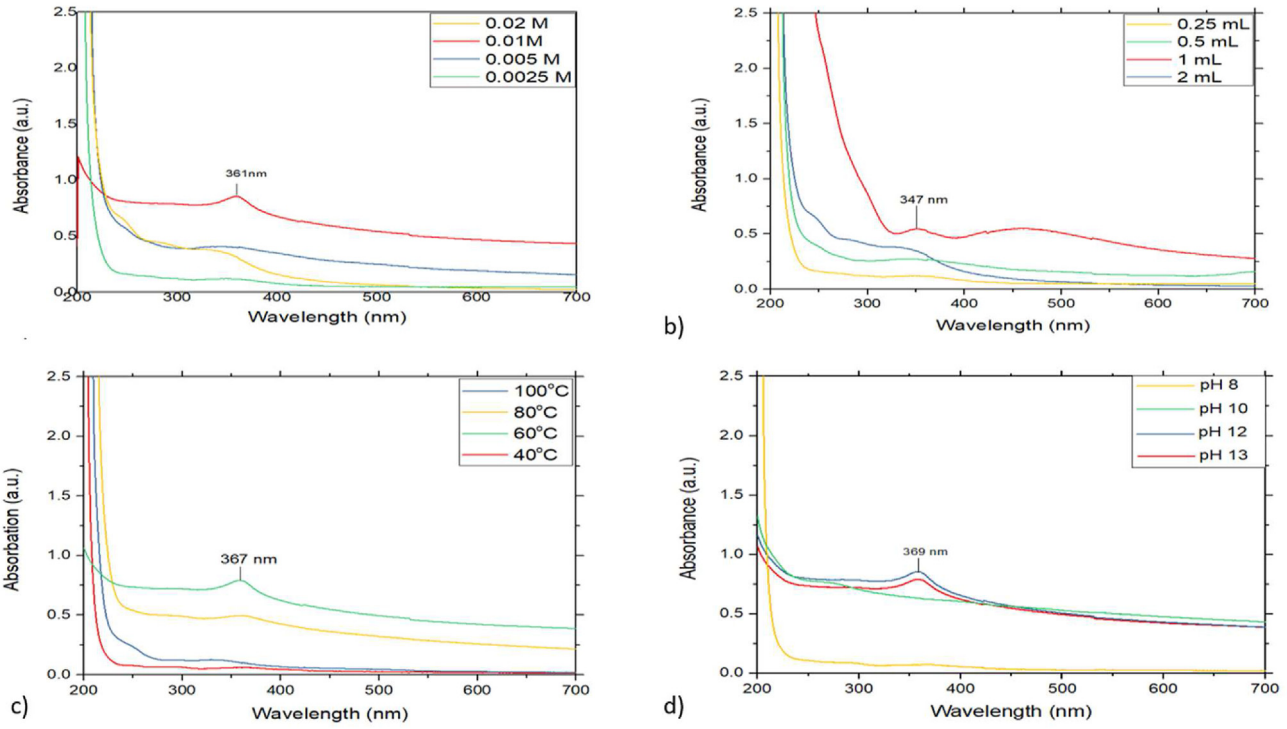

Figure 2. Optimization of synthesis parameters for bio-synthesis of ZnO NPs: (a) Molarity of zinc acetate; (b) Plant leaf extract volume; (c) Temperature; (d) pH.

3. Results and discussion

3.1. Phenotypic, biochemical and molecular characterization of the clinical uropathogenic bacterial isolates

All the eight collected uropathogenic bacterial isolates were characterized phenotypically, biochemically and at the molecular level. Through Gram staining, all the eight isolates were confirmed as Gram-negative, which were further identified using IMViC biochemical tests (Table 2) as tentatively belonging to *Escherichia, Klebsiella, Pseudomonas,* and *Shigella spp*.

The confirmatory identification of all eight uropathogenic bacterial isolates was carried out by amplifying and sequencing the 16S rRNA gene. Upon amplification of the 16S rRNA gene, DNA bands of nearly 1500bp were obtained (Figure 1), which were further examined after their sequencing. With the aid of BioEdit software, the consensus sequences were obtained, and homology with the already existing sequences in the NCBI databases was determined through the BLASTn tool. The accession numbers (Table 2) were obtained by submitting the confirmed 16SrRNA sequences of all uropathogenic bacterial strains to the GenBank Database. The eight uropathogens were identified as four strains of *Klebsiella pneumoniae* (MT444767, MT444769, MT444771, and MT444773), and one strain each of *Escherichia furgusonii* (MT444768), *Shigella flexneri* (MT444770), *Pseudomonas aeruginosa* (MT444772), and *Escherichia coli* (OK035230).

3.2. Antibiotic susceptibility analysis of clinical uropathogenic bacterial isolates

The antibiotic susceptibility profiling was performed by using a set of 23 different antibiotics, which mainly belonged to the following five classes: (i) β-lactams, (ii) β-lactamase inhibitors, (iii) Fluoroquinolones, (iv) Aminoglycosides, and (v) a few other antibiotics (belonging to nitrofurans, sulfonamides, glycylcyclines and polymyxins) used for the treatment of UTIs. In the present study, all eight uropathogens were observed to be resistant to twenty or more than 20 antibiotics, except one strain of *Klebsiella pneumoniae* (MT444769), which was found to exhibit resistance against nineteen antibiotics (Table 3). The uropathogens demonstrated 100% resistance towards β-lactams including penicillin, cefalosporins, carbapenems; towards beta-lactam inhibitors, and also against fluoroquinolones, and aminoglycosides, except for amikacin, for which resistance was observed to be 50% (Table 4). Among the antibiotics other than the above four major classes, 100% resistance was exhibited by the tested uropathogenic bacterial isolates for cotrimoxazole (sulfonamide), and 75% resistance against fosfomycin. For nitrofurantoin (nitrofuran), the isolates exhibited 62.5% resistance, as three strains of *Klebsiella pneumoniae* (MT444767, MT444769, and MT444773) were found to be sensitive to nitrofurantoin. Tigecycline (glycylcycline) and colistin (polymyxin) were observed to be the only effective antibiotics against the tested uropathogens; however, even against these, one strain of *Klebsiella pneumoniae* (MT444771) was found to be resistant (Table 4).

Our findings are in harmony with several other studies [14, 27, 32, 33], wherein it has been reported that *E. coli* has shown a high degree of resistance against cephalosporins and quinolone groups of antibiotics; however, being sensitive to amikacin, nitrofurantoin and fosfomycin,. In a similar kind of study, UPECs have been reported to exhibit 84.7% resistance to ampicillin (penicillin), but 93.6% susceptiblity to nitrofurantoin [33]. Similarly, *Klebsiella pneumoniae* has also been reported to exhibit a high resistance to all the antibiotic groups, but showing susceptibility to tigecycline and colistin. Although *Enterobacteriaceae spp.* have been reported to exhibit a high degree of resistance to fluoroquinolones, but, a previous study has shown that 90.6% of *Enterobacteriaceae spp.* are sensitive to amikacin, and 84.4% to nitrofurantoin; and approximately 70% *Pseudomonas aeruginosa* are sensitive to piperacillin/tazobactam [32]. Hence, for the antibiotics, nitrofurantoin, fosfomycin, and tigecycline, the UTI causing pathogens have been reported to be susceptible enough [27]. However, contrary to this, in the present study 100% resistance was observed by *Pseudomonas aeruginosa* and one strain of *Klebsiella pneumoniae* to most of these antibiotics.

Thus, several studies have described and concluded that UTI-causing uropathogens show a high degree of resistance to all the four major classes of antibiotics (β-lactams, β-lactamase inhibitors, fluoroquinolones, andaminoglycosides except amikacin); whereas, only a few antibiotics such as colistin, fosfomycin, nitrofurantoin, tigecycline and amikacin have been reported to be effective for use as drugs against uropathogens [14].

3.3. Optimization of biosynthesis of ZnO nanoparticles

The bio-synthesis of ZnO NPs was optimised using various abiotic parameters, *viz.* concentration, volume of the plant extract, temperature, and pH. In the present examination, it was observed that an increase in the concentration of zinc acetate from 0.0025 M up to 0.01 M resulted in

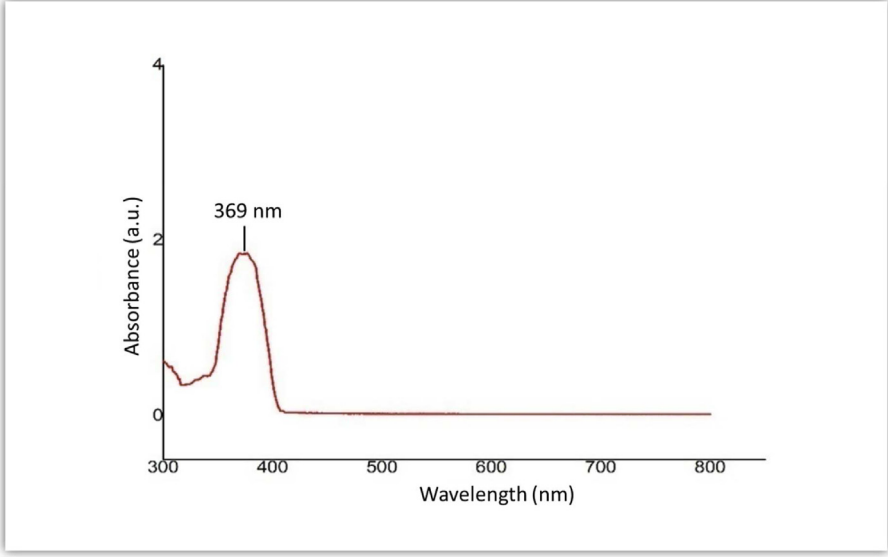

Figure 3. UV-Vis spectra of synthesized ZnO nanoparticles.

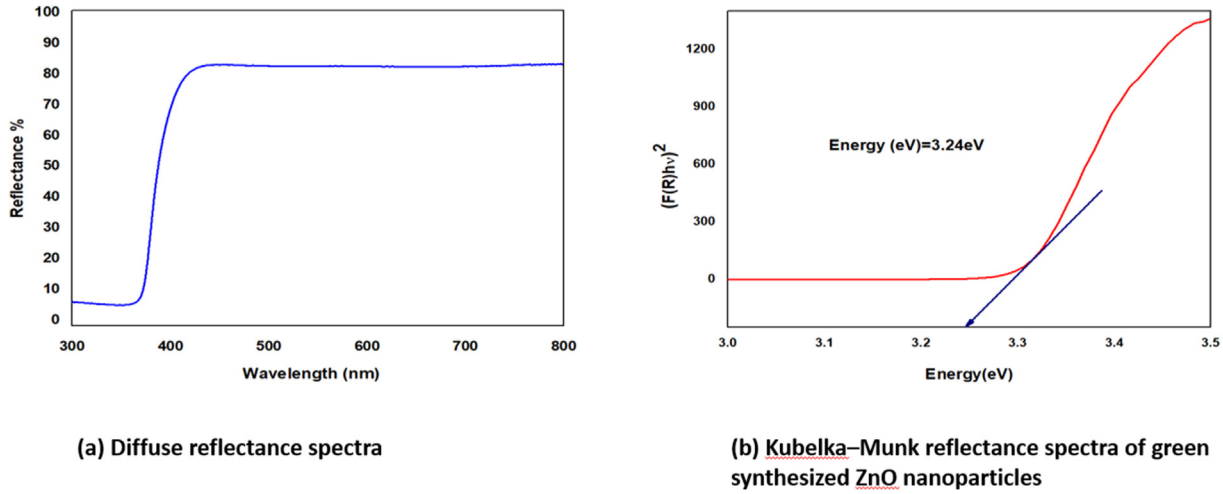

Figure 4. (a) Diffuse reflectance % spectra of synthesized ZnO nanoparticles, and (b) Optical band gap obtained from Kubelka-Munk function and Energy (eV) for synthesized ZnO nanoparticles.

a sharp absorbance; however, a decrease in absorbance was recorded with the widening of the peak at 0.02M concentration, revealing that a further increase in concentration after this threshold limit led to a decrease in absorption, depicting a declining trend in the synthesis of nanoparticles (Figure 2a). Similarly, upon evaluating different concentrations of the plant leaf extract (0.25 ml, 0.50 ml, 1 ml and 2 ml), the maximal absorption was found to be at 1 ml of the leaf extract when 50 ml of zinc acetate was used. It was noted that a further increment or reduction in this volume of the plant leaf extract resulted in a decrease in absorption and further in the biosynthesis of nanoparticles (Figure 2b).

Other significant factors involved in the biosynthesis of ZnO NPs included temperature and pH. In the present study, ZnO NP synthesis was optimised at various temperatures (ranging from 40 °C to 100 °C) (Figure 2c). No prominent synthesis was observed at 40 °C, as depicted by a straight absorption line. Maximum absorption with a sharp peak at 367 nm was observed at 60 °C, while a reduction in absorbance and broadening of the peak was observed at 80 °C. A further increment in temperature led to a sharp decrease in absorbance with no mark of a prominent peak at 100 °C. This may be attributed to the fact that biomolecules of the plant which help in reduction and stabilization of synthesized nanoparticles, get denatured at high temperatures, resulting in the absence of synthesis and in turn loss of the absorbance peak.

The pH is also considered as an important factor in the biosynthesis of ZnO NPs. In the present work, almost a straight line of absorption with no prominent peak was observed at pH 8; whereas an increase in absorption was observed from pH 10 to pH 12, and a sharp peak at 369 nm was observed at pH 12. It was also examined that with a further increase in pH to 13, a decline in absorption was noted (Figure 2d). Hence, it could be concluded that the optimum conditions for the synthesis of ZnO NPs included the preparation of a mixture of 0.01 M zinc acetate, and a concentration involving 1 ml of leaf extract in 50 ml of zinc acetate, at a temperature and pH of 60 °C and 12, respectively.

In a similar kind of study, it has been reported that an increase in concentration resulted in steady absorption with a prominent synthesis of ZnO NPs; however, a further increase in concentration after 0.01 M depicting a reduction in absorption, and finally, a decline in ZnO NPs synthesis. Similarly, while employing various plant leaf extract concentrations, the maximum absorption with a sharp peak has been reported at 1ml. During optimisation of pH studies, a better synthesis has been reported at pH 12, the sharp absorption peaks being observed at both pH 12 and 13 [34]. While in the present study, it has been observed that with an increase in pH after a threshold value of pH 12, a decrease in absorption takes place. In the case of temperature, in the present study, maximum absorption with a sharp peak was observed at 60 °C, whereafter a further increase in temperature resulted in a reduction in absorption, and therefore, in the synthesis of metal oxides. However, contrary to this, in a previous study, it was examined that the maximum absorption for the synthesis of metal oxide nanoparticles was observed at 90 °C [34].

3.4. Physiochemical characterization of biosynthesized ZnO nanoparticles

3.4.1. UV-visible spectroscopy analysis

UV-Vis spectroscopy is often performed for the initial confirmation of nanoparticle synthesis. In the present study, a sharp absorption peak obtained at 369nm clearly marked the bio-synthesis of *B. pinnatum* leaf extract mediated ZnONPs (Figure 3). Similar peaks have been reported in earlier studies also, where different plant parts like the flower extract of *Nyctanthes arbor-tristis*, leaf extract of *Justicia procumbense* and the shell extract *of Punica granatum* have been exploited to produce ZnO nanoparticles, wherein sharp absorption peaks at 365 nm, 370 nm and 370 nm, respectively, have been reported [34, 35, 36, 37].

Further, the reflectance spectra of the biosynthesized ZnO NPs were examined to estimate their optical band gap (Figure 4a). The reflectance spectra exhibited a substantial reduction at 440 nm, as shown in Figure 4(a). This reduction could be corresponded to the electron transition taking place in the optical band gap. The reflectance (R) measurements were converted to absorbance using the Kubelka-Munk function $[F(R)h\upsilon]^2$ in order to calculate the band gap value by using Kubelka-Munk equation:

$$[F(R)h\upsilon]^2 = [1 - R^2 / R] * h\upsilon^2$$

The direct band gap of synthesized ZnO NPs was calculated from the plot of $(F(R)h\upsilon)^2$ versus the photon energy ($h\upsilon$), and the value was obtained as 3.24 eV (Figure 4b). Other scientists have also reported the band gap values of 3.10 eV, and 3.21 eV for ZnO nanoparticles [29, 38].

3.4.2. FTIR analysis

FTIR spectroscopy is performed to get specific signals obtained by substance-specific vibrations of molecules. FTIR spectra determine the various functional moieties engaged in synthesizing ZnO NPs within a range of 4000–500 cm^{-1}. To examine the function of aqueous leaf extract of *Bryophyllum pinnatum* in reducing and stabilizing the nanoparticles, Attenuated Total Reflection-Fourier Transform Infrared spectroscopy (ATR-FTIR) studies were carried out. For this, the FTIR spectra of control salt (zinc acetate), ZnO NPs and *Bryophyllum pinnatum* plant leaf extract was analyzed.

The FTIR spectra of control salt demonstrated various peaks in the range of 3315.38 to 640.49 cm^{-1} at 3315.38, 2135.11, 1625.71, 1456.94 and 640.49 cm^{-1}. The broad peak corresponding to 3315.38 and

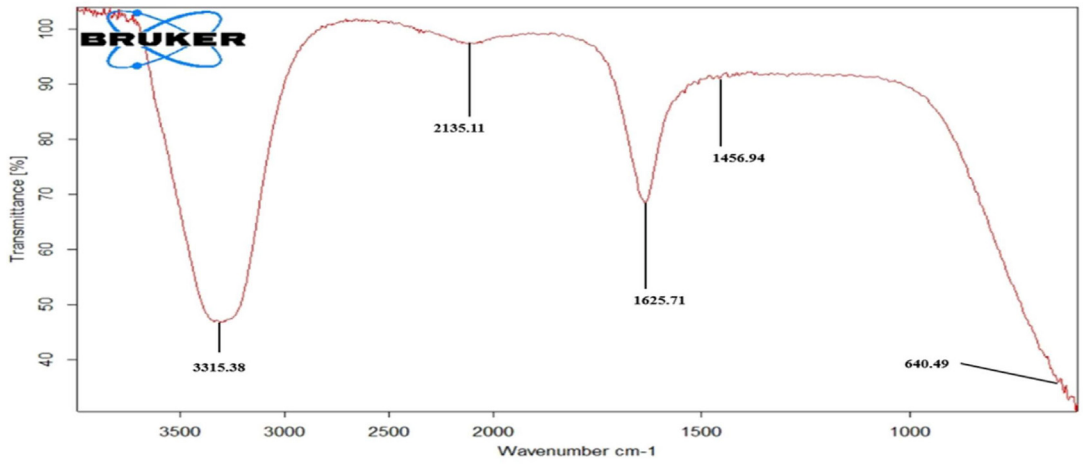

(a)

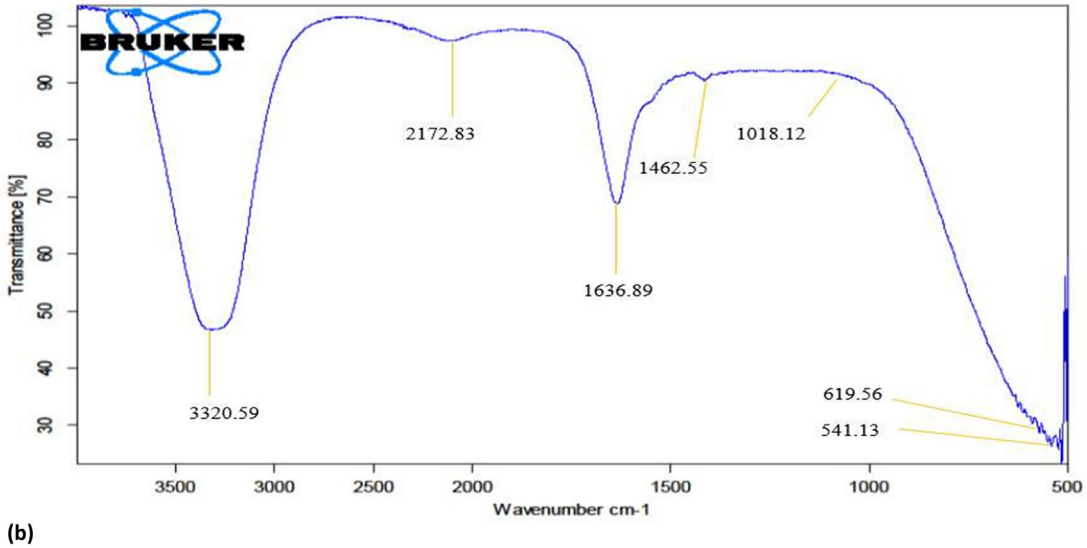

(b)

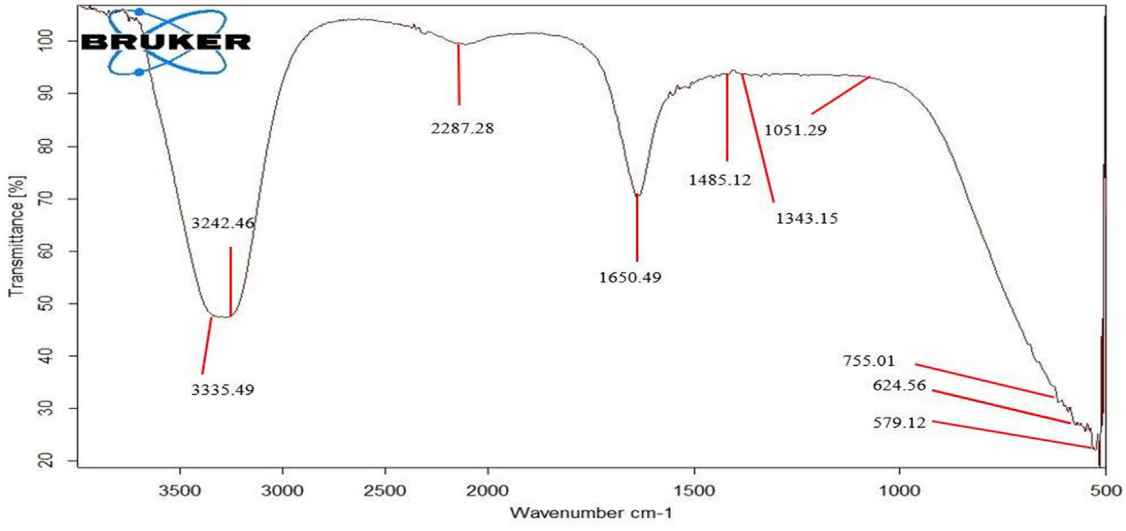

(c)

Figure 5. FTIR spectra of (a) Control salt (Zinc acetate); (b) Synthesized ZnO nanoparticles; and (c) *Bryophyllum pinnatum* leaf extract.

Table 5. Functional moieties of control salt (Zinc acetate), ZnO NPs and *Bryophyllum pinnatum* leaf extract as analyzed by ATR-FTIR.

	Control salt (Zinc acetate)		ZnO NPs		*Bryophyllum pinnatum* leaf extract	
S.No	Absorption Peaks (cm^{-1})	Functional Moieties/Bond	Absorption Peaks (cm^{-1})	Functional Moieties/Bond	Absorption Peaks (cm^{-1})	Functional Moieties/Bond
1	3315.38	H bonded O–H vibrations	3320.59	H bonded O–H vibrations	3335.49; 3242.46	H bonded O–H stretch vibrations
2	2135.11	C≡C stretch vibrations	2172.83	C≡C stretch vibrations	2287. 28	C≡C stretch vibrations
3	1625.71	C=O stretching	1636.89	C=O stretching	1650.49	C=O stretching vibrations
4	1456.94	amine –NH vibration stretch corresponds to protein amides	1462.55	amine –NH vibration stretch corresponds to protein amides	1485.12	amine –NH vibration stretch corresponds to protein amides
5	-	-	-	-	1343.15	Aromatic amines
6	-	-	1018.12	C–N stretch of aliphatic amines	1051.29	C–N stretch of aliphatic amines
7	-	-	-	-	755.01	Alkanes
8	640.49	C- Alkyl chloride	619.56	C- Alkyl chloride	624.56	C- Alkyl chloride
9	-	-	541.13	Hexagonal phase ZnO	579.12	C–Br vibrational stretch

2135.11 was attributed to H-bonded O–H vibrations and C≡C stretch vibrations. The peaks at 1625.71, 1456.94 and 640.49 were attributed to C=O stretching, amine –NH vibrational stretch of protein amide linkages and C- Alkyl chloride vibrations (Figure 5a).

On the other hand, ZnO NPs (Figure 5b) resulted in a slightly larger number of peaks in the range of 3320 to 542 cm^{-1}, at 3320.59, 2172.83, 1636.89, 1462.55, 1018.12, 619.56 and 541.13 cm^{-1}. While FTIR spectra of *Bryophyllum pinnatum* plant leaf extract (Figure 5c) resulted into peaks in the range of 3335 to 580 cm^{-1}, at 3335.49, 3242.46, 2287.28, 1650.49, 1485.12, 1343.15, 1051.29, 755.01, 624.56, and 579.12 cm^{-1}. This shift in the range of peaks could be attributed to the capping of biochemical components of the plant onto ZnO for the reduction and stabilization required during the green synthesis of metal oxide nanoparticles. The broad peak obtained in the FTIR spectra of ZnO-NPs (Table 5) at 3320.59 could be attributed to H-bonded O–H vibrations of the bio-synthesized NPs [4, 34]. The peaks at 2172.83 and 1636.89 corresponded to C≡C stretch and C=O stretching vibrations, respectively. The peak at 1462.55 was attributed to an amine –NH vibration stretch present in the protein amide linkages. The weak peak of 1018.12 resulted from the C–N stretch of aliphatic amines. The peaks obtained at 619.56 and 541.13 were attributed to the C- Alkyl chloride and hexagonal phase of ZnO [4, 39].

The plant leaf extract demonstrated immense peaks (Figure 5c) and (Table 5) at 3335.49, 3242.46, which could be attributed to H-bonded O–H stretch and N–H stretching vibrations (probably exhibited by the presence of alcohols and phenols) [3]. The peak obtained at 2287.28 corresponded to the C≡C stretch [40], whereas the peaks 1650.49, 1485.12, and 1343.15 were attributed to C=O stretching and C=C aromatic stretch vibrations, protein amide linkages and aromatic amines [24, 41, 42]. The peak obtained at 1051.29 and 755.01 corresponded to the C–N stretch of aliphatic amines and alkanes [34]. The peaks at 624.56 and 579.12 were attributed to C- Alkyl chloride and the C–Br vibrational stretch [4].

By comparing the FTIR spectra of the control salt, ZnO NPs and that of plant leaf extract, it was found that a few bands which were observed in ZnO NPs, were not present in the precursor salt, but were found in the plant leaf extract. The FTIR results show that the green synthesized ZnO NPs have an additional band (corresponding to the C–N stretch of aliphatic amines (1018.12) and another band at 541.13 which may be attributed to hexagonal phase of ZnO); both these bands were not present in the control salt (zinc acetate). However, the plant leaf extract comprised of both these bands (1051.29 attributed to the stretch of aliphatic amines and 579.12 to C–Br vibrations). This indicates the role of plant biomolecules in the synthesis of ZnO NPs, most probably as reducing and stabilizing agents. It has been reported earlier also that the existence of the OH group in the flavonoids of plant leaf extract is responsible for the synthesis of ZnO NPs, and the presence of protein molecules in the plant leaf extract are accountable for reducing and stabilizing biosynthesized nanoparticles by playing the role as NPs capping agent [43, 44, 45]. Upon comparing the peaks between the synthesized ZnO NPs and the plant leaf extract, it was observed that all

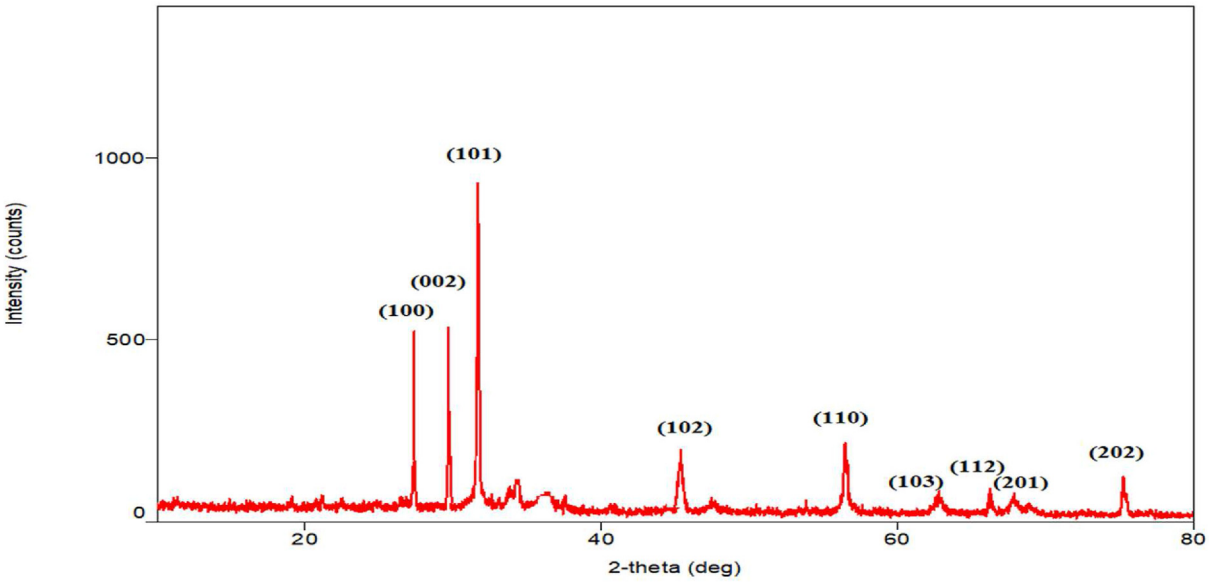

Figure 6. XRD spectra of synthesized ZnO nanoparticles.

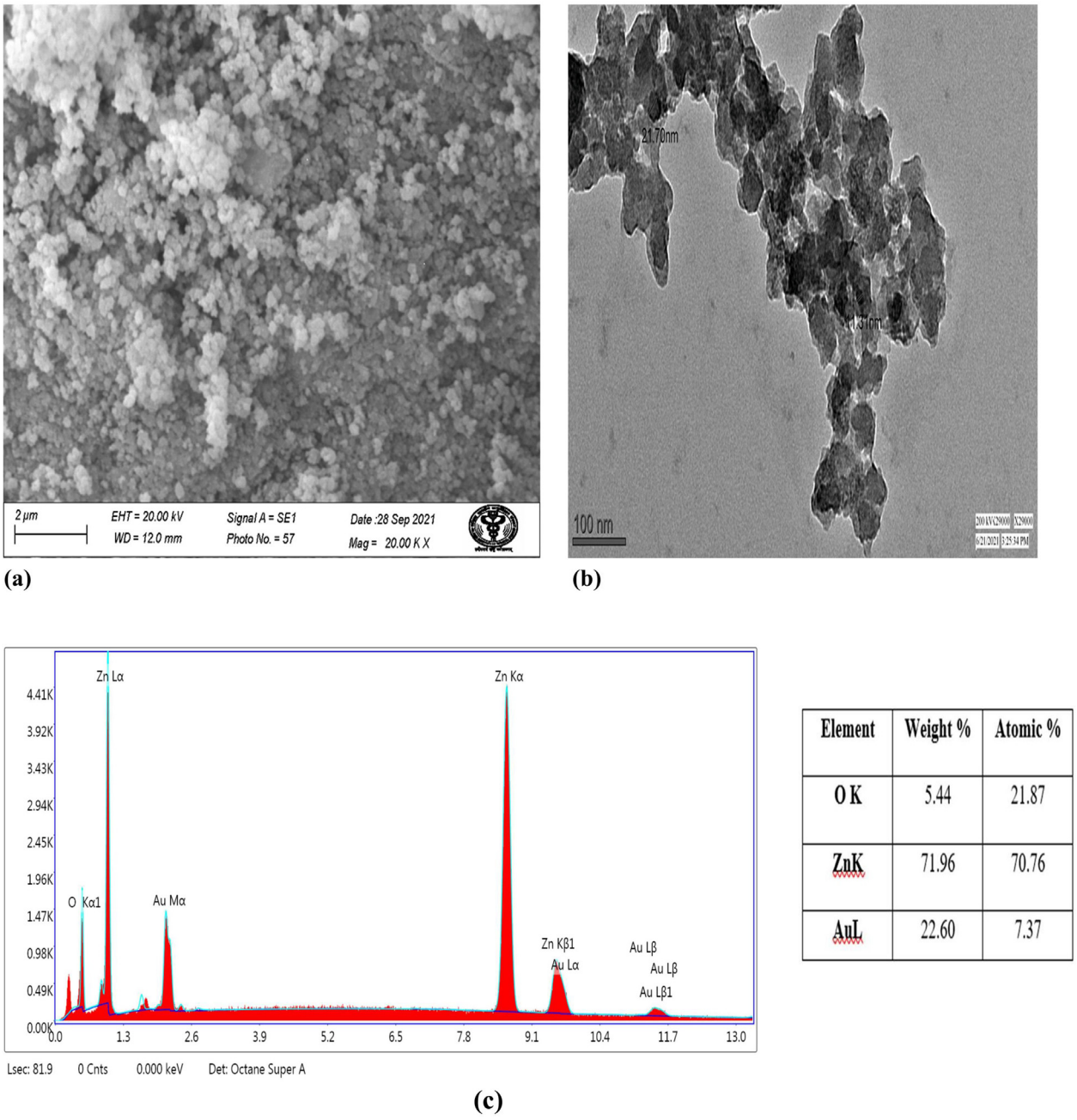

Element	Weight %	Atomic %
O K	5.44	21.87
ZnK	71.96	70.76
AuL	22.60	7.37

Figure 7. (a) SEM; (b) TEM; and (c) EDX image of synthesized ZnO NPs.

the peaks present in the FTIR spectra of the plant leaf extract exhibited a deviation involving a drop in the frequency and a reduction in intensity when bound with the nanoparticles. Hence, it could be concluded that the *Bryophyllum pinnatum* plant leaf extract plays an important role in reducing and stabilizing the synthesis of ZnO NPs, and hence the process of synthesis of ZnO NPs adopted in the present study represents the green methodology approach.

3.4.3. XRD analysis

The XRD spectra provided the structural and crystallinity information of the synthesized ZnO green nanoparticles (Figure 6). In this, strong diffraction peaks of 2θ values were obtained at 31.66°, 34.31°, 36.16°, 45.40°, 56.44°, 62.70°, 66.22°, 67.65° and 75.26°. The peculiar Bragg reflections were indexed at a position of (100), (002), (101), (102), (110), (103), (112), (201) and (202) crystal planes, and were observed to be wurtzite hexagonal phase of ZnO, which is in conformity with Joint Committee on Powder Diffraction Standards (JCPDS file 36–1451). Similar results have been reported by other scientists in previous studies as well [34, 35, 39, 46].

By using Bragg's Law equation: $\mathbf{n\lambda = 2dsin\theta}$ (where λ is X-Ray wavelength, n is 1, and θ is Bragg's angle of diffraction), the interplanar d-spacing was calculated. XRD has been performed to observe the crystallite size. The crystallite size was further estimated with the aid of the Debye-Scherrer equation: $\mathbf{D = 0.9\ \lambda/\beta\ cos\ \theta}$, where 0.9 = Scherrer's constant, β is Full Width at Half Maximum (FWHM) located at peak 2θ = 36.16°, and θ is Bragg's angle of diffraction against an intense peak corresponding to (101) plane [34]. The integral width of the sample (B sample) was analysed by finding the ratio of the area and the height of the peak, and it was observed to be 0.60 (degree). XRD affirmed the crystallite size to be 19.83 nm.

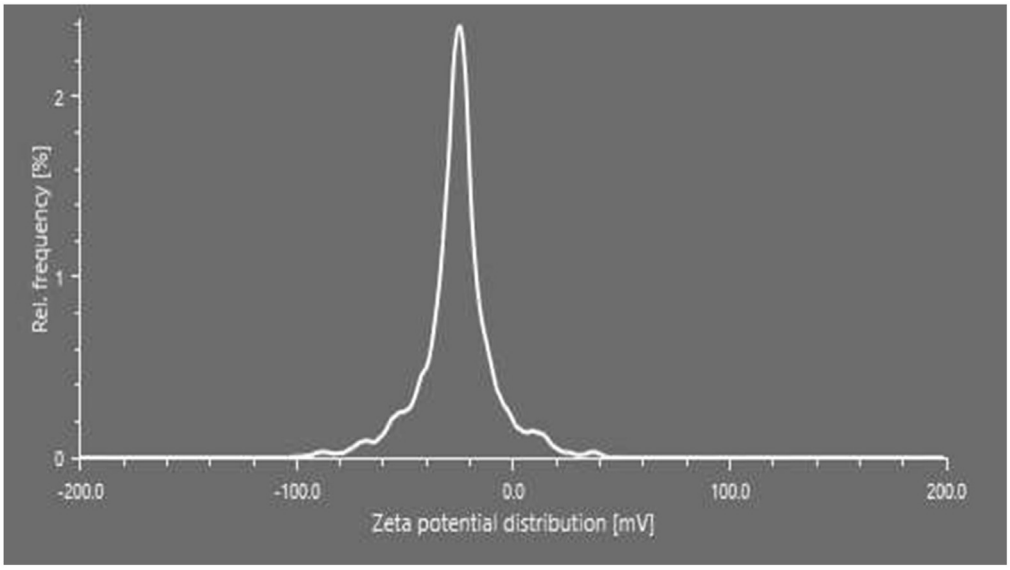

Figure 8. Zeta Potential of synthesized ZnO nanoparticles.

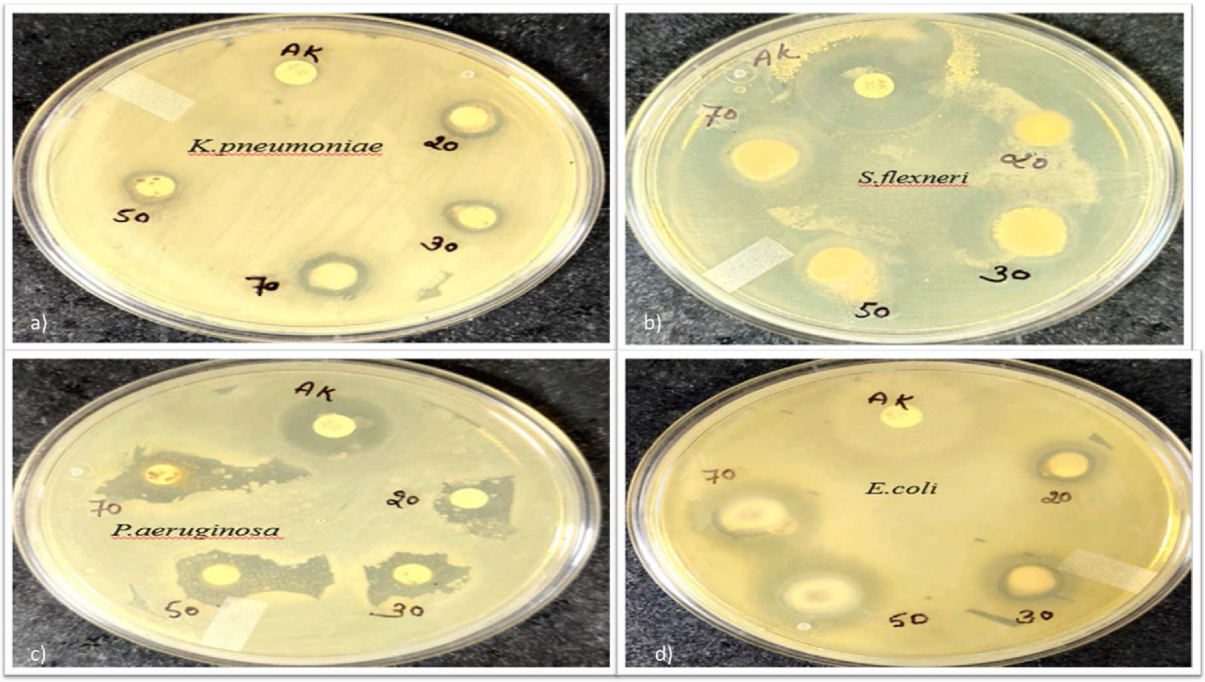

Figure 9. Antibacterial activity of ZnO NPs against (a) *K. pneumoniae;* (b) *S. flexneri;* (c) *P. aeruginosa;* and (d) *E. coli.*

3.4.4. SEM, HR-TEM, and EDX analysis

The size, morphology and form of the synthesized ZnO nanoparticles were evaluated using Scanning electron microscopy (SEM). Figure 7(a) depicts the SEM image of the bio-synthesized nanoparticles, which were spherical and slightly agglomerated. The diameter of the nanoparticles was found to be 5–18 nm. Some previous studies have also reported the bio-synthesized ZnO NPs having spherical shapes with an average size of 5–15 nm and a diameter of 20–40 nm [35, 47].

High-resolution TEM analysis affirmed the morphology and size of bio-synthesized NPs. Figure 7(b) represents the HR-TEM image of the biosynthesized ZnO nanoparticles, which were observed to be quasi-spherical in shape within a size range of 11–35 nm. The average size was observed to be 22.57 nm. The size of nanoparticles was observed to be in good harmony with that of XRD analysis, wherein the crystallite size was observed to be 19.83 nm. In a previous similar study, the green synthesis methodology using *Agathosma betulina* leaf extract has reported quasi-spherical shaped ZnO NPs having an average size of 19.4 nm [48]. The synthesis of ZnO nanoparticles by employing *Anisochilus carnosus* leaf extract has also been reported to result in quasi-spherical shaped nanoparticles with sizes in the range of 30–40 nm [47].

EDX analysis determined the elemental composition of synthesized ZnO NPs, revealing the presence of 71.96 % of Zn, 5.44% of O and 22.60% of Au (Figure 7c), which affirms the purity of synthesized nanoparticles. The presence of Au was observed, as it was used as the coating material for EDX examination. The calculated theoretical ratio of the Zn/O was found to be 4.088%. The theoretical weight % of oxygen and zinc was found to be 19.65% and 80.34%, whereas experimental weight % for both the elements were found to be 21.87% and 70.76%,

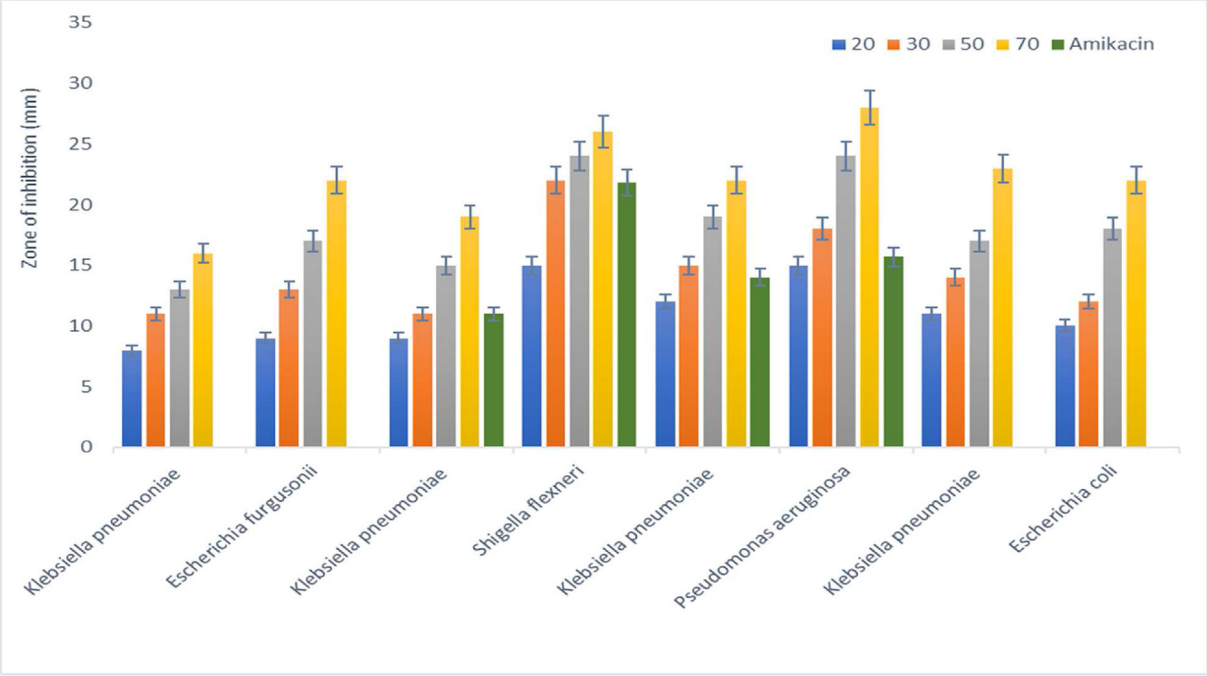

Figure 10. Bar diagram representing the antibacterial ability of bio-synthesized ZnO nanoparticles (at varying concentrations) against clinical MDR uropathogens.

Table 6. Antibacterial ability and minimum inhibitory concentration (MIC) of ZnO NPs against clinical MDR uropathogens.

S.No	Isolate Name	Identified Microorganism	Zone of Inhibition (mm±SD)					MIC of ZnO NPs (μg/ml)
			Synthesized ZnO NPs (μg/ml)				Amikacin (μg)	
			20	30	50	70	30	
1	F26	*K. pneumoniae*	8.00 ± 0.4	11 ± 0.2	13 ± 0.28	16 ± 0.06	No zone	64
2	F32	*E. furgusonii*	9.00 ± 0.1	13 ± 0.08	17 ± 0.08	22 ± 0.12	No zone	64
3	H33	*K. pneumoniae*	9.00 ± 0.04	11 ± 0.08	15 ± 0.05	19 ± 0.08	11.6 ± 0.20	32
4	N39	*S. flexneri*	15 ± 0.03	22 ± 0.17	24 ± 0.44	26 ± 0.06	21.8 ± 0.11	16
5	N40	*K. pneumoniae*	12 ± 0.08	15 ± 0.17	19 ± 0.14	22 ± 0.17	14 ± 0.23	16
6	P27	*P. aeruginosa*	15 ± 0.06	18 ± 0.06	24 ± 0.2	28 ± 0.11	15.7 ± 0.14	16
7	H42	*K. pneumoniae*	11 ± 0.08	14 ± 0.11	17 ± 0.14	23 ± 0.17	No zone	32
8	H11	*E. coli*	10 ± 0.08	12 ± 0.13	18 ± 0.06	22 ± 0.08	No zone	64

respectively. Other studies have also revealed a similar elemental composition of ZnO nanoparticles [37, 46, 47, 49, 50].

3.4.5. Analysis of zeta potential

Another analytical technique, *viz.*, zeta potential, analysed the surface charge's potentiality of the bio-synthesized nanoparticles. The net value of the surface charge of the synthesized nanoparticles was found to be −24.9 mV (Figure 8), showing that the synthesized NPs are relatively durable with a lesser tendency to show aggregation. The zeta potential values with dimensions ˂−30 and ˃+30 are considered extraordinarily stable, having lesser probabilities of forming agglomerations because of a better rate of repulsion among particles [31]. In similar studies, the stability of synthesized nanoparticles was analysed with lesser zeta potential values of −18.4 mV and −15.3 mV [49, 51]. Hence, from the present work, it could be stated that with controlled and optimised synthesis conditions, better stability of nanoparticles can be achieved by employing the green synthesis methodology.

3.5. Analysis of the antibacterial potential of bio-synthesized ZnO nanoparticles

The agar disc diffusion method was employed to analyse the efficacy of the antibacterial ability of the bio-formulated ZnO nanoparticles against clinical MDR Gram-negative uropathogens (Figure 9). ZnO NPs were observed to show intense antibacterial activity in a dose-established manner. An increase in ZnO NPs concentration was observed to be directly proportionate to the antibacterial ability (Figure 10). The levels of zonations were obtained within the range of 08–28 mm, and the maximum antimicrobial efficacy was found to be against *Pseudomonas aeruginosa* (28 ± 0.11 mm), followed by against *Shigella flexneri* (26 ± 0.06 mm), *Klebsiella pneumoniae* (23 ± 0.17 mm), *E. furgusonii* (22 ± 0.12), and *E. coli* (22 ± 0.08 mm). Thus, the synthesized ZnO NPs were found to be bestowed with strong antimicrobial ability against all the tested MDR uropathogens (Table 6, Figures 9 and 10).

In the present study, amikacin, a type of aminoglycoside, one of the most potent antibiotics commonly used for the treatment of UTIs, was used as the control for comparative evaluation of the antimicrobial potential of biosynthesized nanoparticles. Amikacin was observed to exhibit maximum inhibition of bacterial growth for *S. flexneri* (21.8 ± 0.11), followed by that of *P. aeruginosa* (15.7 ± 0.14), and two strains of *K. pneumonia* (14 ± 0.23 and 11.6 ± 0.20). This response of amikacin (inhibition zones in the range of 11–21 mm) was quite less as compared to the antibacterial activity exhibited by the ZnO-NPs even at a concentration as low as 30 μg/ml. Further, four MDR uropathogens, *viz.*, *E. furgusonii* (MT444768), *K. pneumonia* (MT444773), *E. coli* (OK035230) and *K. pneumonia* (MT444767) were observed to be 100% resistant to

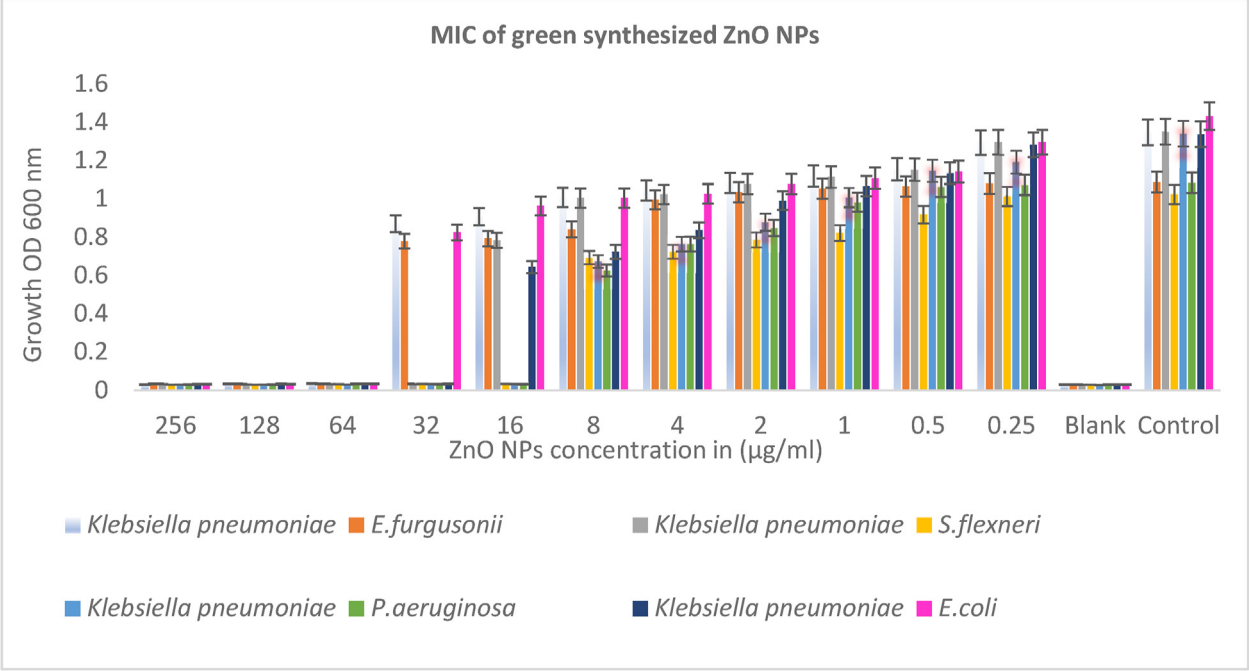

Figure 11. Bar diagram representing the MIC of ZnO nanoparticles against clinical MDR uropathogens at OD600 nm.

amikacin; however, the synthesized ZnO-NPs were found to be effective against these even at concentrations of 20 µg/ml. Hence, from the present study, it could be concluded that the bio-synthesized ZnO NPs have better antimicrobial potential than the current commonly used empiric antibiotic therapy against the MDR uropathogens. A similar study had been conducted earlier using *Berberis aristata* leaf extract-mediated ZnO NPs synthesis, wherein antimicrobial activity was reported against two uropathogens *viz., E. coli* (13.0 ± 0.0 mm) and *K. pneumoniae* (15.0 ± 0.2 mm) [30]. On similar lines, the phyto-biomolecule mediated formation of ZnO nanoparticles using leaf extract of *P. caerulea* L. was carried out by another group, who also reported the antibacterial ability of the synthesized nanoparticles against urinary pathogens, including *E. coli* (13.00 mm ± 1.16 mm) and *Klebsiella* sp. (11.00 mm ± 1.16 mm) at a maximum volume of 75 µl of nanopowder solution [4]. It has also been reported that date pulp waste (DPW)- mediated ZnO NPs have good antibacterial activity against *Pseudomonas aeruginosa* (18.4 mm) [52].

Zinc oxide nanoparticles are, therefore, evolving as new antimicrobial compounds, and they exhibit various inhibitory effects on bacterial cells via different mechanisms, including reactive oxygen species (ROS), involving O=O (singlet oxygen), dihydrogen dioxide, and hydroxyl radicals, which ultimately result in bacterial cell death [53]. The production of oxidative stress due to these miniature particles depends on the scale and concentration. ROS come into contact with the bacterial plasma membrane and disrupt its structure, resulting in altered permeability. Such an altered permeability of the plasma membrane results into bulging and suspension of intracellular materials; intruding various substantive/core processes vital for cell maturation and ultimately resulting into the death of the pathogenic bacteria [54]. When cations make a strong bonding with the negative charge of the microbial cells, vital destruction to microbial cells has been reported, as the cations cease the functioning of ribosomes by impairing the functionality of enzymes. It has also been studied that the formation of H_2O_2 within the outer membrane of the bacterial cells is due to an electrical O_2 reaction resulting in the production of O^{2-} radicals. The O^{2-} species are crucial for damaging the bacterial cell lipid or protein molecules [55, 56, 57, 58].

Minimum inhibitory concentration (MIC) values of the synthesized ZnO NPs against the tested eight MDR uropathogens (Table 6 and Figure 11) were determined using both visual turbidity analysis and determination of turbidity via measuring absorbance at OD600 nm. The MIC was observed to be the least for *P. aeruginosa, K. pneumoniae* (MT444771) and *S. flexneri* (16 µg/ml), followed by two strains of *K. pneumonia* which showed growth suppression at 32 µg/ml. *E. furgusonii, E. coli,* and *K. pneumonia* (MT444767) exhibited the highest MIC value at 64 µg/ml. However, these values are quite less when compared to the doses in which the antibiotics are generally used to treat several infections including UTI. In a previous study, *Berberis aristata* leaf extract-mediated ZnO NPs have shown that the synthesized NPs exhibited MIC at a value of 256 µg/ml against *E. coli and K. Pneumonia* [30], which is relatively high as compared to the results obtained in the present study. Hence, it could be inferred that the ZnO NPs synthesized in the present study exhibited a much higher efficacy than the control antibiotic, and the ZnO NPs reported in earlier studies.

4. Conclusion

The imprudent usage of antibiotics has resulted in the upsurge of an era of antimicrobial resistance that has resulted in the production of multidrug-resistant pathogens. Such MDR pathogens hinder the conventional empiric antibiotic therapy and ring an alarm for researcher communities to look for an alternate therapy to cure several infections. In the past few decades, the scientific community has been fascinated by exploring and evolving green chemistry to produce nanoparticles because of its environment-friendly and practical methodology. The presence of phytochemicals in the green sources act as a conjugating operative that helps reduce, stabilize, and further facilitate the shape and size-controlled nanoparticle synthesis. The present study comprised the facile green methodology for synthesising ZnO nanoparticles *via Bryophyllum pinnatum* leaf extract and characterization of these NPs for their antibacterial ability against highly MDR urinary tract infection causing uropathogens. The bio-synthesized nanopowder was characterized by employing many analytical approaches: UV-Vis spectroscopy, DRS, XRD and FTIR spectroscopy, SEM, HR-TEM, EDX, and zeta potential. UV-Vis spectroscopy affirmed the formation of ZnO NPs at a sharp absorption peak of 369nm. FTIR spectroscopy revealed the conjugation of plant phytochemicals with ZnO NPs that played a pivotal role in reducing and stabilizing them. XRD spectroscopy affirmed the crystallinity and wurtzite hexagonal phase of ZnO NPs. Additionally, SEM and HR-TEM

revealed the exact morphology and size of the biosynthesized NPs. Zeta potential analysis confirmed the relatively stable and lesser agglomerative nature of synthesized nanoparticles. The antimicrobial assay demonstrated the strong antimicrobial efficacy possessed by ZnO NPs against the tested MDR uropathogens, *viz. E. coli, K. pneumoniae, P. aeruginosa, E. furgusonii* and *S. flexneri*. The antibacterial assay results have revealed that phytochemically fabricated nanoparticles can be utilized for evolving future nanoantibiotics against the MDR uropathogens. And the present study is a step forward in the evolvement of nano-based antibiotics.

Declarations

Author contribution statement

Kiran Nehra: Conceived and designed the experiments; Contributed reagents, materials, analysis of tools or data.

Renu Jagdish: Performed the experiments; Analyzed and interpreted the data; Wrote the paper.

Funding statement

This research did not receive any specific grant from funding agencies in the public, commercial, or not-for-profit sectors.

Data availability statement

Data will be made available on request.

Declaration of interest's statement

The authors declare no conflict of interest.

Additional information

No additional information is available for this paper.

Acknowledgements

The authors are thankful to the Sophisticated Analytical Instrument Facility (SAIF) AIIMS for providing SEM, EDX and HR-TEM facilities. The authors are also grateful to Central Instrumentation Facility (CIF), Jamia Millia Islamia University, Delhi, for providing the XRD facility.

References

[1] N.M. Ngoepe, Z. Mbita, M. Mathipa, N. Mketo, B. Ntsendwana, N.C. Hintsho-Mbita, Biogenic synthesis of ZnO nanoparticles using Monsonia burkeana for use in photocatalytic, antibacterial and anticancer applications, Ceram. Int. 44 (2018) 16999–17006.

[2] H. Agarwal, S.V. Kumar, S. Rajeshkumar, A review on green synthesis of zinc oxide nanoparticles–An eco-friendly approach, Resour. Technol. 3 (2017) 406–413.

[3] P. Rajiv, S. Rajeshwari, R. Venckatesh, Bio-Fabrication of zinc oxide nanoparticles using leaf extract of Parthenium hysterophorus L. and its size-dependent antifungal activity against plant fungal pathogens, Spectrochim. Acta Part A Mol. Biomol. Spectrosc. 112 (2013) 384–387.

[4] J. Santhoshkumar, S.V. Kumar, S. Rajeshkumar, Synthesis of zinc oxide nanoparticles using plant leaf extract against urinary tract infection pathogen, Resour. Technol. 3 (2017) 459–465.

[5] M. Gupta, R.S. Tomar, S. Kaushik, R.K. Mishra, D. Sharma, Effective antimicrobial activity of green ZnO nano particles of Catharanthus roseus, Front. Microbiol. 9 (2018) 2030.

[6] K.V. Dhandapani, D. Anbumani, A.D. Gandhi, P. Annamalai, B.S. Muthuvenkatachalam, P. Kavitha, B. Ranganathan, Green route for the synthesis of zinc oxide nanoparticles from Melia azedarach leaf extract and evaluation of their antioxidant and antibacterial activities, Biocatal. Agric. Biotechnol. 24 (2020), 101517.

[7] M. Bandeira, A.L. Possan, S.S. Pavin, C.S. Raota, M.C. Vebber, M. Giovanela, M. Roesch-Ely, D.M. Devine, J.S. Crespo, Mechanism of formation, characterization and cytotoxicity of green synthesized zinc oxide nanoparticles obtained from Ilex paraguariensis leaves extract, Nano-Struct. Nano-Objects 24 (2020), 100532.

[8] S. cSahin Dougan, A. Kocabacs, Green synthesis of ZnO nanoparticles with Veronica multifida and their antibiofilm activity, Hum. Exp. Toxicol. 39 (2020) 319–327.

[9] S. Vijayakumar, B. Vaseeharan, B. Malaikozhundan, M. Shobiya, Laurus nobilis leaf extract mediated green synthesis of ZnO nanoparticles: characterization and biomedical applications, Biomed. Pharmacother. 84 (2016) 1213–1222.

[10] L.C. Ann, S. Mahmud, S.K.M. Bakhori, A. Sirelkhatim, D. Mohamad, H. Hasan, A. Seeni, R.A. Rahman, Antibacterial responses of zinc oxide structures against Staphylococcus aureus, Pseudomonas aeruginosa and Streptococcus pyogenes, Ceram. Int. 40 (2014) 2993–3001.

[11] P. Vanathi, P. Rajiv, S. Narendhran, S. Rajeshwari, P.K.S.M. Rahman, R. Venckatesh, Biosynthesis and characterization of phyto mediated zinc oxide nanoparticles: a green chemistry approach, Mater. Lett. 134 (2014) 13–15.

[12] G. Sangeetha, S. Rajeshwari, R. Venckatesh, Green synthesis of zinc oxide nanoparticles by aloe barbadensis miller leaf extract: structure and optical properties, Mater. Res. Bull. 46 (2011) 2560–2566.

[13] M.S. Kumar, A.P. Das, Emerging nanotechnology based strategies for diagnosis and therapeutics of urinary tract infections: a review, Adv. Colloid Interface Sci. 249 (2017) 53–65.

[14] S. Malik, J.S. Rana, K. Nehra, others, Prevalence and antibiotic susceptibility pattern of uropathogenic *Escherichia coli* strains in sonipat region of Haryana in India, Biomed, Biotechnol. Res. J. 5 (2021) 80.

[15] M. Khoshkbejari, A. Jafari, M. Safari, Ag/ZnO nanoparticles as novel antibacterial agent against of Escherichia coli infection, in vitro \& in vivo, Orient, J. Chem. 31 (2015) 1437–1445.

[16] L.K. McLellan, D.A. Hunstad, Urinary tract infection: pathogenesis and outlook, Trends Mol. Med. 22 (2016) 946–957.

[17] A. Bryce, A.D. Hay, I.F. Lane, H. V Thornton, M. Wootton, C. Costelloe, Global prevalence of antibiotic resistance in paediatric urinary tract infections caused by Escherichia coli and association with routine use of antibiotics in primary care: systematic review and meta-analysis, Bmj 352 (2016).

[18] H. Giamarellou, G. Poulakou, Multidrug-resistant gram-negative infections, Drugs 69 (2009) 1879–1901.

[19] P.-R. Hsueh, W.-H. Chen, K.-T. Luh, Relationships between antimicrobial use and antimicrobial resistance in Gram-negative bacteria causing nosocomial infections from 1991–2003 at a university hospital in Taiwan, Int. J. Antimicrob. Agents. 26 (2005) 463–472.

[20] M. Bodro, G. Sanclemente, I. Lipperheide, M. Allali, F. Marco, J. Bosch, F. Cofan, M.J. Ricart, N. Esforzado, F. Oppenheimer, others, Impact of antibiotic resistance on the development of recurrent and relapsing symptomatic urinary tract infection in kidney recipients, Am. J. Transplant. 15 (2015) 1021–1027.

[21] B.A. Aderibigbe, Metal-based nanoparticles for the treatment of infectious diseases, Molecules 22 (2017) 1370.

[22] A. Sultan, H.M. Khan, A. Malik, A. Ansari, A. Azam, N. Perween, Antibacterial activity of ZnO nanoparticles against ESBL and Amp-C producing gram negative isolates from superficial wound infections, Int. J. Curr. Microbiol. App. Sci. 1 (2015) 38–47.

[23] M. Afzal, I. Kazmi, R. Khan, R. Singh, M. Chauhan, T. Bisht, F. Anwar, Bryophyllum pinnatum: a review, Int. J. Res. Biol. Sci 2 (2012) 143–149.

[24] A. Latif, K. Ashiq, S. Ashiq, E. Ali, I. Anwer, S. Qamar, others, Phytochemical analysis and in vitro investigation of anti-inflammatory and xanthine oxidase inhibition potential of root extracts of Bryophyllum pinnatum, J. Anim. Plant Sci 30 (2020) 219–228.

[25] K. Nehra, N. Chhabra, P.K. Sidhu, P. Lathwal, J.S. Rana, Molecular identification and characterization of Poly-$β$hydroxybutyrate (PHB) producing bacteria isolated from contaminated soils, Asian J. Microbiol. Biotechnol. Environ. Sci. 17 (2017) 281–290.

[26] D. Prakash, R.S. Saxena, Distribution and antimicrobial susceptibility pattern of bacterial pathogens causing urinary tract infection in urban community of meerut city, India, Int. Sch. Res. Not. 2013 (2013).

[27] M.A. Lawhale, R. Naikwade, Recent pattern of drug sensitivity of most commonly isolated uropathogens from Central India, Int. J. Res. Med. Sci 5 (2017) 3631–3636.

[28] M.P. Weinstein, J.B. Patel, A.M. Bobenchik, S. Campeau, S.K. Cullen, M.F. Gallas, Clinical and laboratory standards institute, Perform. Stand. Antimicrob. Susceptibility Test, 2019, pp. 88–89.

[29] H.S. Lalithamba, M. Raghavendra, K. Uma, K.V. Yatish, D. Mousumi, G. Nagendra, Capsicum annuum fruit extract: a novel reducing agent for the green synthesis of ZnO nanoparticles and their multifunctional applications, Acta Chim. Slov. 65 (2018) 354–364.

[30] H. Chandra, D. Patel, P. Kumari, J.S. Jangwan, S. Yadav, Phyto-mediated synthesis of zinc oxide nanoparticles of Berberis aristata: characterization, antioxidant activity and antibacterial activity with special reference to urinary tract pathogens, Mater. Sci. Eng. C. 102 (2019) 212–220.

[31] P.K. Sidhu, K. Nehra, Bacteriocin-capped silver nanoparticles for enhanced antimicrobial efficacy against food pathogens, IET Nanobiotechnology 14 (2020) 245–252.

[32] P. Mehrishi, S.S. Faujdar, S. Kumar, S. Solanki, A. Sharma, others, Antibiotic susceptibility profile of uropathogens in rural population of Himachal Pradesh, India: where We are heading? Biomed. Biotechnol. Res. J. 3 (2019) 171.

[33] A.R.S. Va, S. Shenoy, R.M. Taruna Yadav, The antibiotic susceptibility patterns of uropathogenic Escherichia coli, with special reference to the fluoroquinolones, J. Clin. Diagnostic Res. JCDR. 7 (2013) 1027.

[34] P. Jamdagni, P. Khatri, J.S. Rana, Green synthesis of zinc oxide nanoparticles using flower extract of Nyctanthes arbor-tristis and their antifungal activity, J. King Saud Univ. 30 (2018) 168–175.

[35] S. Umavathi, M. Ramya, C. Padmapriya, K. Gopinath, Green synthesis of zinc oxide nanoparticle using Justicia procumbense leaf extract and their application as an antimicrobial agent, J. Biol. Act. Prod. from Nat. 10 (2020) 153–164.

[36] E. Karaköse, H. Çolak, F. Duman, Green synthesis and antimicrobial activity of ZnO nanostructures Punica granatum shell extract, Green Process. Synth. 6 (2017) 317–323.
[37] K. Elumalai, S. Velmurugan, Green synthesis, characterization and antimicrobial activities of zinc oxide nanoparticles from the leaf extract of Azadirachta indica (L.), Appl. Surf. Sci. 345 (2015) 329–336.
[38] J. Estrada-Urbina, A. Cruz-Alonso, M. Santander-González, A. Méndez-Albores, A. Vázquez-Durán, Nanoscale zinc oxide particles for improving the physiological and sanitary quality of a Mexican landrace of red maize, Nanomaterials 8 (2018) 247.
[39] K. Viswanathan, I. Kim, G. Kasi, K. Sadeghi, S. Thanakkasaranee, J. Seo, Facile approach to enhance the antibacterial activity of ZnO nanoparticles, Adv. Appl. Ceram. 119 (2020) 414–422.
[40] A.M. Kolo, S. Idris, O.M. Bamishaiye, Corrosion inhibition potential of ethanol extract of Bryophyllum pinnatum leaves for zinc in acidic medium, Edelweiss Appl. Sci. Technol. 2 (2018) 18–25.
[41] D. Ebere Okwu, F. Uchenna Nnamdi, A novel antimicrobial phenanthrene alkaloid from Bryopyllum pinnatum, E-J. Chem. 8 (2011) 1456–1461.
[42] N. Legner, C. Meinen, R. Rauber, Root differentiation of agricultural plant cultivars and proveniences using FTIR spectroscopy, Front. Plant Sci. 9 (2018) 748.
[43] J. Fowsiya, I. V Asharani, S. Mohapatra, A. Eshapula, P. Mohi, N. Thakar, S. Monad, G. Madhumitha, Aegle marmelos phytochemical stabilized synthesis and characterization of ZnO nanoparticles and their role against agriculture and food pathogen, Green Process. Synth. 8 (2019) 488–495.
[44] M. Naseer, U. Aslam, B. Khalid, B. Chen, Green route to synthesize Zinc Oxide Nanoparticles using leaf extracts of Cassia fistula and Melia azadarach and their antibacterial potential, Sci. Rep. 10 (2020) 1–10.
[45] A.D. Jadhao, S. Shende, P. Ingle, A. Gade, S.W. Hajare, R.S. Ingole, Biogenic synthesis of zinc oxide nanoparticles by Bryophyllum pinnatum and its acute oral toxicity evaluation in wistar rats, IEEE Trans. Nanobioscience. 19 (2020) 633–639.
[46] K. Ali, S. Dwivedi, A. Azam, Q. Saquib, M.S. Al-Said, A.A. Alkhedhairy, J. Musarrat, Aloe vera extract functionalized zinc oxide nanoparticles as nanoantibiotics against multi-drug resistant clinical bacterial isolates, J. Colloid Interface Sci. 472 (2016) 145–156.
[47] M. VannanAnbu, M. Ramesh, G. Viruthagiri, N. Shanmugam, N. Kannadasan, Anisochilus carnosus leaf extract mediated synthesis of zinc oxide nanoparticles for antibacterial and photocatalytic activities, Mater. Sci. Semicond. Process. 39 (2015) 621–628.
[48] F.T. Thema, E. Manikandan, M.S. Dhlamini, M. Maaza, Green synthesis of ZnO nanoparticles via Agathosma betulina natural extract, Mater. Lett. 161 (2015) 124–127.
[49] M. Abinaya, B. Vaseeharan, M. Divya, A. Sharmili, M. Govindarajan, N.S. Alharbi, S. Kadaikunnan, J.M. Khaled, G. Benelli, Bacterial exopolysaccharide (EPS)-coated ZnO nanoparticles showed high antibiofilm activity and larvicidal toxicity against malaria and Zika virus vectors, J. Trace Elem. Med. Biol. 45 (2018) 93–103.
[50] S. Fakhari, M. Jamzad, H. Kabiri Fard, Green synthesis of zinc oxide nanoparticles: a comparison, Green Chem. Lett. Rev. 12 (2019) 19–24.
[51] E. Selvarajan, V. Mohanasrinivasan, Biosynthesis and characterization of ZnO nanoparticles using Lactobacillus plantarum VITES07, Mater. Lett. 112 (2013) 180–182.
[52] K. Rambabu, G. Bharath, F. Banat, P.L. Show, Green synthesis of zinc oxide nanoparticles using Phoenix dactylifera waste as bioreductant for effective dye degradation and antibacterial performance in wastewater treatment, J. Hazard. Mater. 402 (2021), 123560.
[53] N. Padmavathy, R. Vijayaraghavan, Enhanced bioactivity of ZnO nanoparticles—an antimicrobial study, Sci. Technol. Adv. Mater. (2008).
[54] L. Zhang, Y. Jiang, Y. Ding, M. Povey, D. York, Investigation into the antibacterial behaviour of suspensions of ZnO nanoparticles (ZnO nanofluids), J. Nanoparticle Res. 9 (2007) 479–489.
[55] S. Shaheen, A. Iqbal, M. Ikram, M. Imran, S. Naz, A. Ul-Hamid, A. Shahzadi, W. Nabgan, J. Haider, A. Haider, Graphene oxide-ZnO nanorods for efficient dye degradation, antibacterial and in-silico analysis, Appl. Nanosci. (2022) 1–13.
[56] A. Haider, M. Ijaz, M. Imran, M. Naz, H. Majeed, J.A. Khan, M.M. Ali, M. Ikram, Enhanced bactericidal action and dye degradation of spicy roots' extract-incorporated fine-tuned metal oxide nanoparticles, Appl. Nanosci. 10 (2020) 1095–1104.
[57] M. Ikram, A. Mahmood, A. Haider, S. Naz, A. Ul-Hamid, W. Nabgan, I. Shahzadi, J. Haider, I. Ahmad, S. Ali, Dye degradation, antibacterial and in-silico analysis of Mg/cellulose-doped ZnO nanoparticles, Int. J. Biol. Macromol. 185 (2021) 153–164.
[58] M. Ikram, S. Aslam, A. Haider, S. Naz, A. Ul-Hamid, A. Shahzadi, M. Ikram, J. Haider, S.O.A. Ahmad, A.R. Butt, Doping of Mg on ZnO nanorods demonstrated improved photocatalytic degradation and antimicrobial potential with molecular docking analysis, Nanoscale Res. Lett. 16 (2021) 1–16.